

Effective Therapy of Drug-Resistant Bacterial Infection by Killing Planktonic Bacteria and Destructing Biofilms with Cationic Photosensitizer Based on Phosphindole Oxide

Jianqing Li, Zijuan Meng, Zeyan Zhuang, Bingnan Wang, Jun Dai, Guangxue Feng, Xiaoding Lou, Fan Xia, Zujin Zhao,* and Ben Zhong Tang

Developing effective therapies to fight against biofilm-associated infection is extremely urgent. The complex environment of biofilm forces the bacteria to evade the elimination of antibiotics, resulting in recalcitrant chronic infections. To address this issue, a cationic antibacterial agent based on phosphindole oxide (β -PM-PIO) is designed and prepared. The unique molecular structure endows β -PM-PIO with aggregation-induced emission feature and efficient singlet oxygen generation ability. β -PM-PIO shows excellent visual diagnostic function to planktonic bacteria and biofilm. In addition, owing to the synergistic effect of phototoxicity and dark toxicity, β -PM-PIO can achieve superb antibacterial and antibiofilm performance against Gram-positive bacteria with less potential of developing drug resistance. Notably, β -PM-PIO also holds excellent anti-infection capacity against drug-resistant bacteria in vivo with negligible side effects. This work offers a promising platform to develop advanced antibacterial agents against multidrug-resistant bacterial infection.

1. Introduction

Bacterial infection has become one of the greatest threats to human health.^[1] Especially, the abuse of antibiotics can cause the evolution of bacterial genes, leading to the drug-resistant bacteria formation and ultimately the failure of previous drugs.^[2] To make it worse, for natural bacteria, the exponential growth promotes biofilm formation, which will reduce the effectiveness of antimicrobials, and accelerate the generation of bacterial resistance. Generally, biofilm is composed of a series of microbial communities, in which bacteria are adhered to a surface and encapsulated by extracellular polymeric substance (EPS) containing DNA, proteins, lipids, polysaccharide, etc.^[3] The existence of EPS not only provides a physical barrier to prevent the penetration of antibiotics but also utilizes enzymes to degrade or absorb anti-

biotics and makes them inactive.^[4] To address these issues, plentiful researches have been taken to defeat biofilm-associated infection,^[5] such as herbal active compounds,^[6] peptide antibiotics,^[7] lantibiotics,^[8] synthetic chemical compounds,^[9] etc. Among them, antimicrobial peptides (AMPs) have played a significant role in fighting against drug-resistant bacteria, which is based on the membrane disruption mechanism of its cationic portion.^[10] However, the poor stability, complex preparation, and high cost for natural AMPs have seriously hindered their clinical application.^[11] Worse still, the therapeutic effect of AMPs that mainly relies on the cationic moieties to destroy bacterial membranes is extremely limited. Additionally, the visual diagnosis is still unachievable.^[12] Therefore, it persistently propels researchers to develop a more efficient antibacterial and antibiofilm strategy with less potential to promote bacterial evolution or intensify drug resistance.


As a novel treatment modality, photodynamic therapy (PDT) serves as a promising clinical medical means owing to its superior merits, such as spatial-temporal controllability, high efficiency, and noninvasiveness.^[13] In recent years, it has exhibited great potentials in antibacterial treatment, especially against resistant-bacterial infection.^[14] The reactive oxygen species (ROS) generated in the PDT can interact with bacteria and cause oxidative damage to vital cellular components of bacteria.^[4b] As

J. Li, Z. Zhuang, B. Wang, G. Feng, Z. Zhao, B. Z. Tang
State Key Laboratory of Luminescent Materials and Devices
Guangdong Provincial Key Laboratory of Luminescence
from Molecular Aggregates
South China University of Technology
Guangzhou 510640, China
E-mail: mszjzhao@scut.edu.cn

Z. Meng, X. Lou, F. Xia
Engineering Research Center of Nano-Geomaterials of Ministry
of Education
Faculty of Materials Science and Chemistry
China University of Geosciences
Wuhan 430074, China

J. Dai
Department of Obstetrics and Gynecology
Tongji Hospital
Tongji Medical College
Huazhong University of Science and Technology
Wuhan 430074, China

B. Z. Tang
School of Science and Engineering
Shenzhen Institute of Aggregate Science and Technology
The Chinese University of Hong Kong
Shenzhen, Guangdong 518172, China

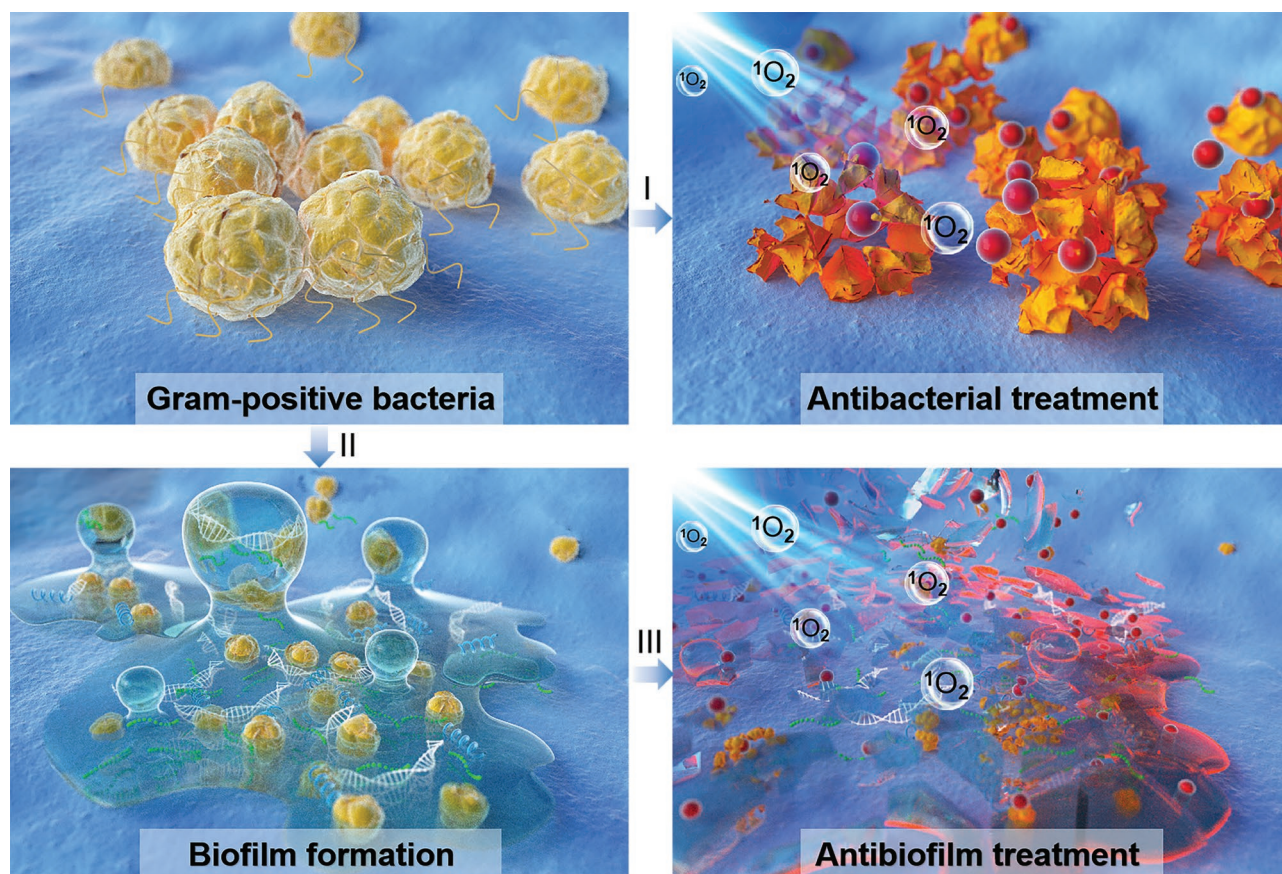
 The ORCID identification number(s) for the author(s) of this article can be found under <https://doi.org/10.1002/smll.202200743>.

DOI: 10.1002/smll.202200743

a key element of PDT, photosensitizers (PSs) directly affect the efficiency of ROS generation.^[15] Notably, the newly developed PSs with aggregation-induced emission (AIE) properties have attracted considerable research interest.^[16] Such kinds of AIE-based PSs tend to aggregate in the biological microenvironment to suppress non-radiative transition, presenting a unique fluorescence “turn on” feature,^[17] which is also beneficial to achieve high ROS generation capacity in aggregates.^[18] In other words, AIE characteristic endows PSs with the functions of accurate diagnosis and effective therapy.^[19] However, the efficacy of PDT is limited by many external conditions (e.g., oxygen and light). Especially in antibiofilm treatment, the light can be scattered by the accumulated bacteria, resulting in an unsatisfactory therapeutic effect. Therefore, stronger conditions are conducive to biofilm treatment, such as higher concentration and longer irradiation time. Considering the excellent antibacterial role of cations in AMPs, it is envisioned that the combination of AIE-based PSs with cations through rational molecular design can achieve improved antibacterial efficiency by the synergistic therapy of phototoxicity and dark toxicity. For one thing, the dark toxicity from cations can compensate the limitation of PDT. For another, the accessorial phototoxicity can reduce the drug doses, bringing about the improved antibacterial effect.

AIE-active cationic PSs based on phosphindole oxide (PIO) hold distinct merits of high electron affinity, satisfactory

photostability, desirable biocompatibility, and excellent ROS generation capacity, which enable them to be promising candidates in antibacterial therapy.^[20] In this contribution, a tailor-made AIE-active cationic antibacterial agent (β -PM-PIO) with photodynamic inactivation activity is prepared, which comprises of triphenylamine (TPA) and thiophene as electron donors, and pyridinium as the electron acceptor. The strong donor-acceptor (D-A) structure of β -PM-PIO is conducive to promoting red-shift of absorption/emission wavelengths as well as enhancing ROS generation. Meanwhile, the introduction of hydrophilic pyridine cation can potentially improve the penetration of β -PM-PIO into the biofilm.^[21] Better, it also endows β -PM-PIO with the bacteria-targeting ability through electrostatic interaction with negatively charged bacterial membranes, to realize visualization for planktonic/biofilm-associated bacteria. Besides the visual function by fluorescence imaging, β -PM-PIO shows excellent antibacterial and antibiofilm capability against Gram-positive bacteria with less potential to develop drug resistance due to the synergistic treatment effect of phototoxicity and dark toxicity (Scheme 1). Moreover, the superior antibacterial performance of β -PM-PIO is also demonstrated in in vivo treatment of methicillin-resistant *staphylococcus aureus* (MRSA)-infected wounds. This work provides an effective strategy for the construction of excellent biofilm detergents and antibacterial agents.



Scheme 1. Illustration of image-guided targeting and synergistic destruction of bacteria and biofilm by AIE-based PS (β -PM-PIO). The processes including: I) Efficient antibiosis by synergistic treatment effect of phototoxicity and dark toxicity; II) the formation of biofilm from planktonic bacteria; III) efficient antibiofilm by the synergistic effect of phototoxicity and dark toxicity.

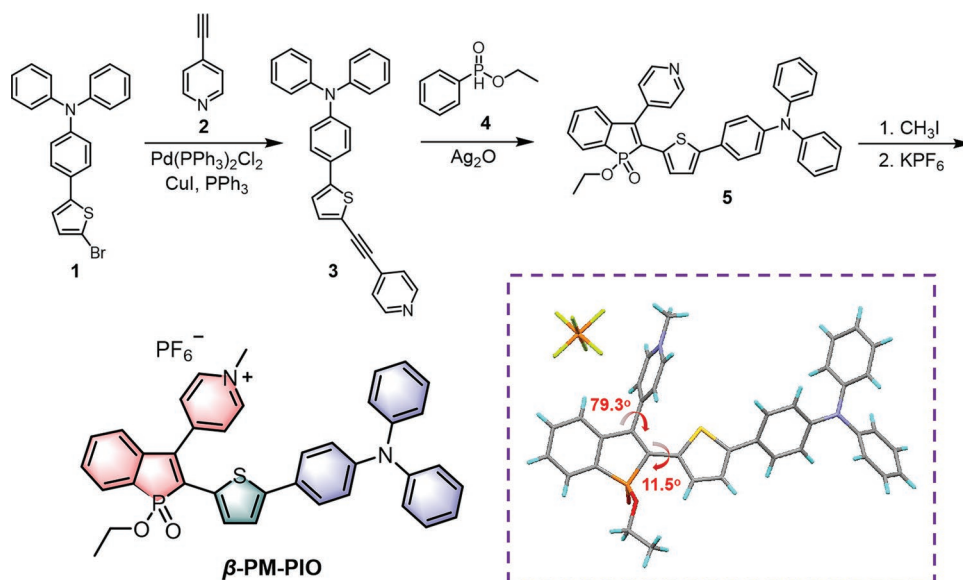


Figure 1. Synthetic route, chemical, and crystal structures of β -PM-PIO.

2. Results and Discussion

2.1. Synthesis and Characterization

The chemical structure of β -PM-PIO and the synthetic route is illustrated in Figure 1. The intermediate 1 is obtained via Suzuki reaction according to the previous literature.^[22] Sonogashira coupling of available 4-ethynylpyridine (2) with 1 gives compound 3, which is cyclized via oxidation under catalyza-tion of silver oxide (Ag_2O) to yield compound 5. The targeted product (β -PM-PIO) is obtained by a two-step reaction of 5, alkylation with methyl iodide, and ion replacement with potassium hexafluorophosphate. Detailed synthetic process and their structural characterizations by nuclear magnetic resonance ($^1\text{H}/^{13}\text{C}$ NMR) and high-resolution mass spectroscopy (HRMS) are given in Supporting Information (Figures S1–S3, Sup-porting Information). Single crystals of β -PM-PIO are obtained in *n*-hexane (hex)/dichloromethane mixture by slow solvent evaporation, and the crystallography analysis further confirms

its chemical structure (Table S1, Supporting Information). As shown in Figure 1, the torsion angle between the thiophene bridge and PIO core is as small as 11.5° , beneficial to improve molecular conjugation. Besides, the nearly vertical connection between pyridinium and PIO core with a large torsion angle of 79.3° can efficaciously facilitate intramolecular charge transfer (CT).^[23]

2.2. Photophysical and ROS Generation Properties

The optical properties of β -PM-PIO are evaluated by absorption and photoluminescence (PL) spectra. It has an obvious absorp-tion band at the region of 350–550 nm with an absorption peak located at 457 nm in dimethyl sulfoxide (DMSO) (Figure 2A), which is associated with the charge transfer from D to A groups. The PL behaviors of β -PM-PIO in the mixtures of tetrahydro-furan (THF)/hex with different hex fractions (f_{hex} s) are meas-ured to confirm its AIE characteristic (Figure 2B; Figure S4,

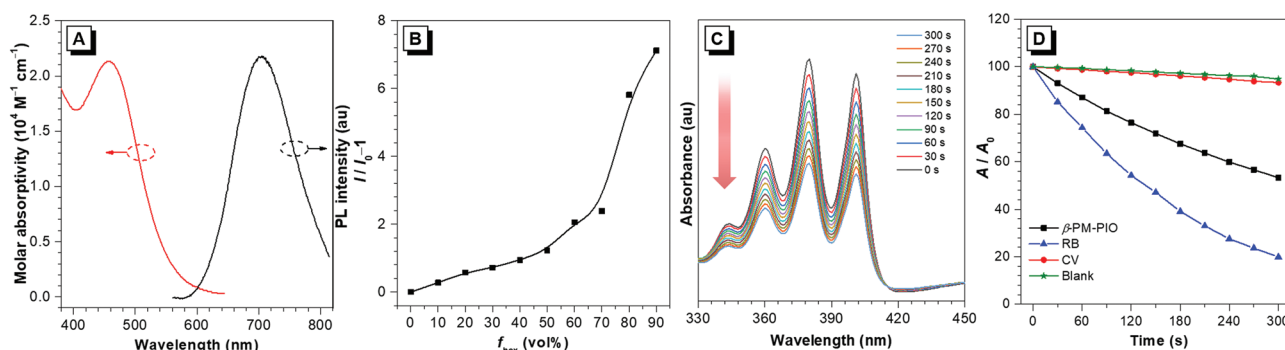


Figure 2. A) Absorption spectrum in pure DMSO and PL spectrum in THF/hex mixture ($f_{\text{hex}} = 90 \text{ vol}\%$) of β -PM-PIO ($\lambda_{\text{ex}} = 480 \text{ nm}$). B) Plots of $I/I_0 - 1$ versus f_{hex} for β -PM-PIO in THF/hex mixtures with different f_{hex} s; I_0 is the PL intensity of the sample in pure THF. C) Photodegradation of ABDA with $10 \mu\text{M}$ β -PM-PIO under white light irradiation (10 mW cm^{-2}) in PBS with $1 \text{ vol}\%$ DMSO. D) Plots of A/A_0 versus irradiation time for the $^1\text{O}_2$ generation of β -PM-PIO ($10 \mu\text{M}$), RB ($10 \mu\text{M}$), CV ($10 \mu\text{M}$), and blank in PBS with $1 \text{ vol}\%$ DMSO using ABDA as indicator under white light irradiation (10 mW cm^{-2}); A_0 is the absorbance of ABDA before irradiation.

Supporting Information). β -PM-PIO barely emits in good solvent (THF), due to that the vigorous intramolecular motions have nonradiatively consumed the excited state energy.^[24] The PL intensity is enhanced with the increase of f_{hex} , indicative of a typical AIE feature. When f_{hex} reaches 90 vol%, β -PM-PIO shows an obvious PL peak at 715 nm (Figure 2A). β -PM-PIO has a higher fluorescence quantum yield at f_{hex} = 90 vol% (2.2%) than that in pure THF (0.6%), which is in accordance with its AIE feature.

In view of its strong absorbance in the visible region, the white light source is employed to trigger the ROS generation of β -PM-PIO in aqueous solution. Firstly, the photostability of β -PM-PIO (10 μM) is evaluated by detecting the variation of the absorbance under white light (10 mW cm^{-2}). The negligible change of the absorption intensity after 20 min irradiation indicates its outstanding stability against photobleaching (Figure S5, Supporting Information). To assess the general ROS generation ability, 2,7-dichlorodihydrofluorescein (DCFH) is used as the indicator.^[25] As displayed in Figure S6A and S7, under white light irradiation (10 mW cm^{-2}) for 3 min, the fluorescence intensity enhances quickly and reaches 217-fold enhancement in the presence of β -PM-PIO, which is higher than those of two commercial PSs (rose Bengal (RB) and crystal violet (CV)). The previously reported PIO-based PSs mainly generate free radical ROS.^[20] This hints us to determine the nature of ROS species of β -PM-PIO via 2-[6-(40-hydroxy) phenoxy-3H-xanthen-3-on-9-yl] benzoic acid (HPF), a commonly used hydroxyl radical ($\text{OH}\cdot$) indicator (Figures S6B and S8, Supporting Information).^[26] However, the fluorescence intensity of HPF is hardly changed within 3 min under the same condition (10 mW cm^{-2}), which urges us to detect the singlet oxygen ($^1\text{O}_2$) generation of β -PM-PIO by 9,10-anthracenediylbis(methylene)dimalonic acid (ABDA), a common $^1\text{O}_2$ probe (Figures 2C,D; Figure S9, Supporting Information).^[27] The $^1\text{O}_2$ quantum yield for β -PM-PIO is 72.5%, tested by using RB as a standard ($\approx 75\%$ quantum yield for $^1\text{O}_2$) (Figure S10, Supporting Information),^[28] strongly evidencing that β -PM-PIO has excellent $^1\text{O}_2$ generation ability.

2.3. Theoretical Calculation

To figure out the working mechanism of the excellent $^1\text{O}_2$ generation for β -PM-PIO, quantum mechanics and molecular mechanics (QM/MM) method with two-layer ONIOM approach is carried on the basis of crystal.^[29] The orbital distributions of the highest occupied molecular orbitals (HOMOs) and the lowest unoccupied molecular orbitals (LUMOs) for β -PM-PIO in the first excited singlet state (S_1) and the first excited triplet state (T_1) are shown in Figure 3A. Owing to the strong electron-donating capacity of TPA and thiophene and strong electron-accepting ability of pyridinium and PIO core, the HOMO is predominantly localized on TPA and thiophene moieties, while the LUMO mainly distributes on pyridinium and PIO core in S_1 state, presenting CT character. In addition, the separation of HOMO and LUMO is favorable for reducing the energy gap (ΔE_{ST}) between S_1 and T_1 states. The ΔE_{ST} of β -PM-PIO in the optimized S_1 state is calculated to be only 0.01 eV (Figure 3B). In T_1 state, the electron clouds of HOMO and LUMO are extended greatly on the entire molecular backbone, indicative of a typical local excitation (LE) character. According to the El-Sayed rule, the effective mixing of the wave functions between ^1CT and ^3LE state is the key to enhance the spin-orbital coupling constant (SOC).^[30] The calculated SOC value between S_1 and T_1 by Dalton is 1.58 cm^{-1} . The small ΔE_{ST} and considerable SOC value can ensure efficient intersystem crossing (ISC) to promote the generation of ROS.^[31]

Moreover, the energy of T_1 state of β -PM-PIO at optimized S_1 state is 1.15 eV, which is higher than the energy required (0.98 eV) to achieve energy transfer from triplet oxygen to $^1\text{O}_2$.^[32] The high T_1 energy level of β -PM-PIO plays a crucial role in the generation of $^1\text{O}_2$ rather than free radical ROS. In addition, the energy transfer process is faster than the electron transfer process, that is to say, β -PM-PIO is more likely to undergo energy transfer to generate $^1\text{O}_2$ under the circumstances.

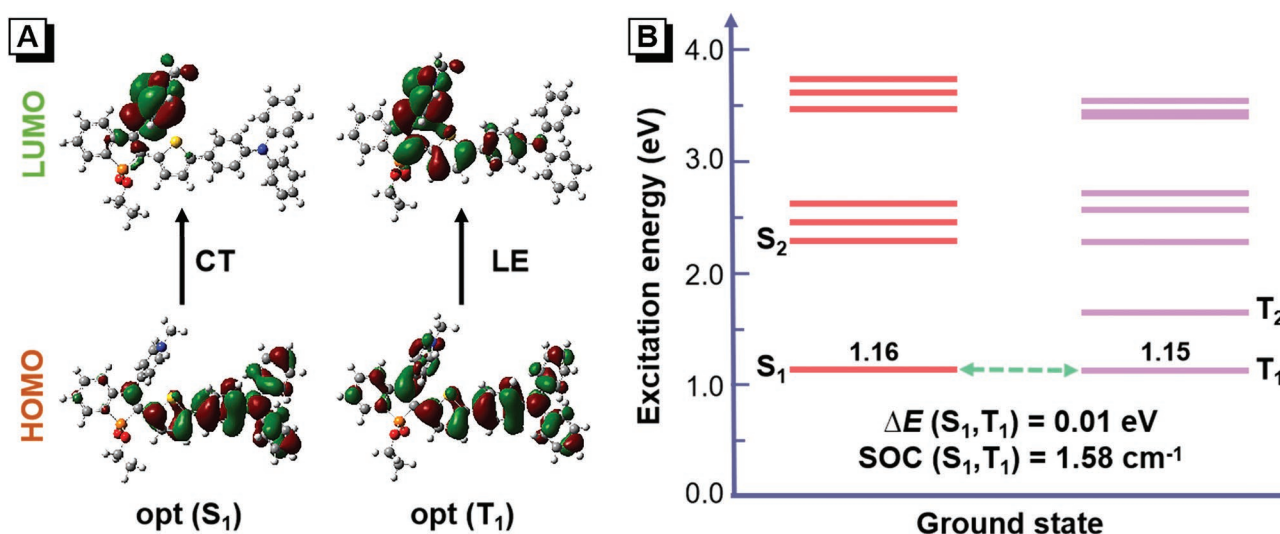


Figure 3. A) HOMOs and LUMOs distributions of β -PM-PIO at the optimized S_1 and T_1 states. B) The energy levels of β -PM-PIO were calculated by the vertical excitation of the optimized S_1 configuration in solid state.

2.4. Bacterial and Biofilm Imaging

Aiming to investigate the imaging ability of β -PM-PIO to planktonic bacteria by confocal laser scanning microscopy (CLSM), Gram-positive bacteria (*S. aureus* and MRSA) and Gram-negative bacteria (*E. coli* and *P. aeruginosa*) are employed as preliminary representative bacteria. The fluorescence images of Gram-positive bacteria incubated with β -PM-PIO (1 μ M) are shown in **Figure 4A**. It can be seen that β -PM-PIO can quickly response to Gram-positive bacteria and shows bright fluorescence upon incubating for 10 min at room temperature (RT). The staining efficiency is as high as nearly 100%. However, *E. coli* can only be partially stained. Yet there is almost no apparent fluorescence signal that can be monitored for *P. aeruginosa*. The binding behavior of β -PM-PIO toward bacteria is then verified via PL spectra (Figure S11, Supporting Information) and zeta potential (ζ) (Figure S12, Supporting Information). After being treated with 5 μ M β -PM-PIO for 10 min at RT, the fluorescence intensity of β -PM-PIO at 670 nm shows nearly 119-fold enhancement in the presence of *S. aureus* and MRSA relative to the blank (5 μ M β -PM-PIO in PBS), but only 67- and 31-fold enhancements in the presence of *E. coli* and *P. aeruginosa*, respectively. In addition to fluorescence intensity, the surface potential alteration for Gram-positive bacteria (3.1–4.3 mV) is more obvious than that for Gram-negative bacteria (0.6–1.4 mV). All of these findings unambiguously manifest that the binding ability of β -PM-PIO with four microbes can be as follows: *S. aureus* \approx MRSA > *E. coli* > *P. aeruginosa*. Such excellent binding affinity towards Gram-positive bacteria may be due to the thick teichoic acid on the outward of bacteria. The binding capacity between cationic β -PM-PIO and anionic lipoteichoic acid (LTA) is evaluated by PL spectra. The obviously enhanced fluorescence in the presence of LTA further confirms that the electrostatic interaction is the main force for the effective bonding between β -PM-PIO and LTA (Figure S13, Supporting Information).^[33]

Afterward, the colocalization experiment is conducted to figure out the interaction site of β -PM-PIO on Gram-positive bacteria (Figures S14A and S14C, Supporting Information). Hoechst 33342, a blue fluorescence probe, is used as the nucleic acid dye of bacteria. As showcased in Figures S14B and S14D,

Supporting Information, the red fluorescence of β -PM-PIO is distributed almost in the whole bacteria. In comparison with the complicated membrane structure of Gram-negative bacteria, amphipathic AIE-active PSs with positive charges are more likely to adhere to the surface and quickly insert into the peptidoglycan membrane of Gram-positive bacteria, rendering an eminent “light up” character.^[34]

To prove the feasibility of β -PM-PIO as an antimicrobial agent, the real-time tracking of the staining process in the mixed HeLa cells and bacteria (*S. aureus* and MRSA) (Figure S15, Supporting Information) is further conducted. Interestingly, once β -PM-PIO (5 μ M) is added, the bacteria are stained quickly. With the extension of coincubation time, the fluorescence intensity is gradually enhanced, but the living cells still cannot be stained after 30 min, demonstrating that β -PM-PIO has the ability to recognize bacteria over mammalian cells. This superior performance is probably ascribed to the higher bacterial membrane potential than cancer cells, which leads to strong electrostatic interaction between positively charged β -PM-PIO and negatively charged bacteria rather than cells.^[35]

Attributing to the selective imaging ability towards planktonic Gram-positive bacteria, the 3D imaging capacity of β -PM-PIO on biofilm is further investigated. And *S. aureus* and MRSA are selected to establish the biofilm models. After static culture of 24 h at 37 °C, 5 μ M β -PM-PIO is added into the petri dish for 10 min at RT. A layer of biofilm with red fluorescence is formed after 24 h (Figure 4B). Furthermore, after extending the culture time to 48 h, the biofilm becomes denser and thicker. As demonstrated above, β -PM-PIO is desirable for planktonic bacteria and biofilm imaging.

2.5. Antibacterial Treatment

Encouraged by the excellent ROS generation and selective targeting ability, the killing capability of β -PM-PIO to planktonic bacteria is further examined. The antibacterial activity is firstly evaluated by a determination of the minimum inhibitory concentration (MIC) against representative bacteria (*S. aureus* and MRSA). After incubating the planktonic bacteria with different concentrations of β -PM-PIO for 30 min, the bacteria are treated

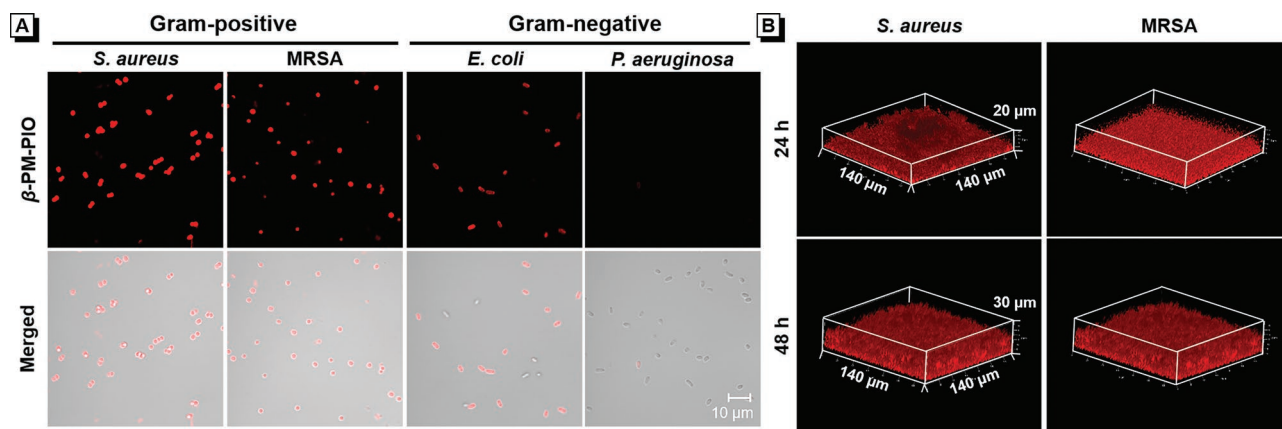


Figure 4. A) CLSM images of *S. aureus*, MRSA, *E. coli*, and *P. aeruginosa* stained with β -PM-PIO (1 μ M) for 10 min at room temperature. B) The 3D CLSM images of *S. aureus* and MRSA biofilms after treatment with β -PM-PIO (5 μ M) for 10 min at room temperature ($\lambda_{\text{ex}} = 488$ nm, $\lambda_{\text{em}} = 600$ –700 nm).

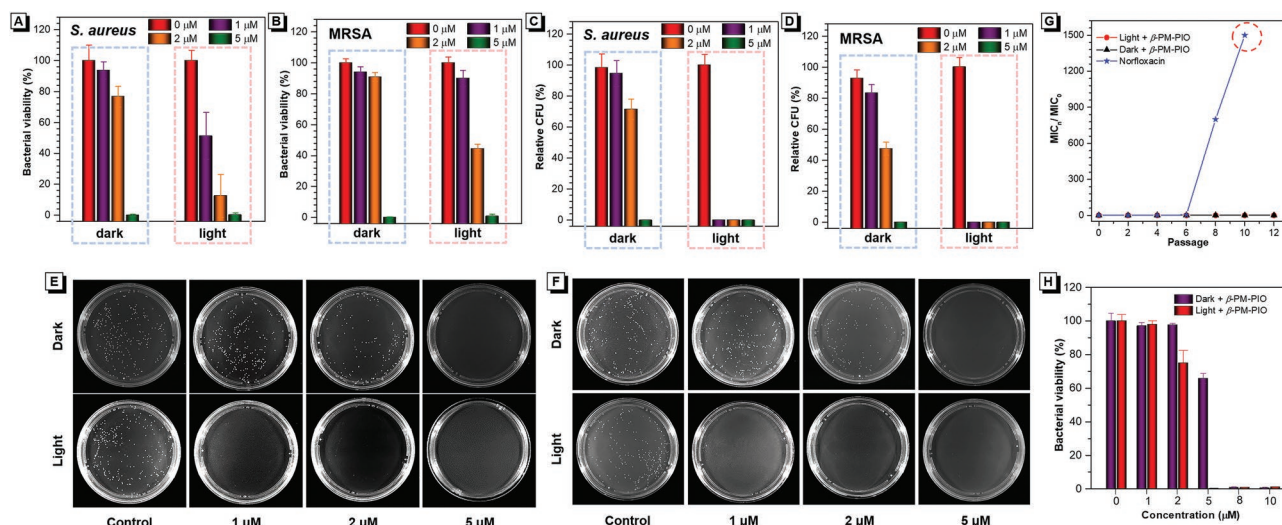


Figure 5. Bacterial viability of A) *S. aureus* and B) MRSA incubated with β -PM-PIO with different concentrations for 16 h in the mixture of culture medium and PBS ($f_{\text{PBS}} = 50 \text{ vol}\%$) under dark and light conditions. Photographs of E) *S. aureus* and F) MRSA treated by β -PM-PIO with different concentrations on the agar plates under dark and light conditions, and the corresponding CFU diagram for C) *S. aureus* and D) MRSA. G) Drug resistance-developing study on *S. aureus* treated by β -PM-PIO and norfloxacin with continues 1/2MIC treatment for 10 generations. MIC_0 is the MIC of the primary passage of *S. aureus*. H) Bacterial viability of the 10th passage norfloxacin-resistant *S. aureus* incubated with β -PM-PIO with different concentrations for 16 h under dark and light conditions. White light: 40 mW cm^{-2} ; 10 min.

with and without white light irradiation (40 mW cm^{-2}) for 10 min, followed by incubation on the shaker in the mixture of culture medium and PBS ($f_{\text{PBS}} = 50 \text{ vol}\%$) for 16 h at 37°C . As displayed in Figure 5A, 5B, and S16, β -PM-PIO shows better antibacterial property against Gram-positive bacteria with an MIC of about $5 \mu\text{M}$, while the MIC against Gram-negative bacteria is more than $10 \mu\text{M}$. These differences are probably due to the discrepant binding ability between bacteria and β -PM-PIO.

Subsequently, the growth curves of Gram-positive bacteria are monitored within 24 h after incubation with different concentrations of β -PM-PIO for 30 min, and then with and without white light irradiation (40 mW cm^{-2}) for 10 min. As shown in Figure S17, *S. aureus* and MRSA appear similarly growth trends after treatment by various concentrations of β -PM-PIO. The growth of *S. aureus* and MRSA can be effectively inhibited at $5 \mu\text{M}$ in both dark and light conditions, indicating its excellent antibacterial effect. Better yet, after exposure to white light (40 mW cm^{-2}) for 10 min, the growth velocity of *S. aureus* and MRSA can be effectively slower at $2 \mu\text{M}$ than that without light illumination. Aiming to further verify its excellent bacterial inactivation, solid agar medium, and live/dead cell imaging are employed. The corresponding colony-forming unit (CFU) counting results on agar plates show that bacterial growth can be completely inhibited at $1 \mu\text{M}$ in the presence of β -PM-PIO (without culture medium) after incubating on the shaker for 30 min and irradiated by white light (40 mW cm^{-2}) for 10 min. However, the concentration should reach $5 \mu\text{M}$ to achieve 100% inhibition efficiency under dark conditions (Figure 5C,D,E,F). Moreover, SYTOX Blue, a dead cell dye, is utilized to test cytoplasmic membrane integrality and mark the dead bacteria. The high coincidence of red fluorescence (β -PM-PIO) and cyan fluorescence (SYTOX Blue) indicates that the bacteria are effectively killed (Figures S18 and S19, Supporting Information). The imaging results are consistent with the plate count method,

indicating β -PM-PIO exhibits efficient phototoxicity in pure PBS culture, and the dark toxicity from cations can enhance its antibacterial effect.

To further understand the antibacterial mechanism of β -PM-PIO, the absorbance at 260 nm is measured to detect cytoplasmic leakage.^[36] As illustrated in Figure S20, *S. aureus*, and MRSA that without any treatment shows ignorable absorbance at 260 nm due to their integrated bacterial membrane. As a comparison, the obviously enhanced absorption at 260 nm after being treated with β -PM-PIO validates the bacterial membrane rupture and bacterial cytoplasmic leakage, highlighting the efficient antibacterial effect resulting from the destruction of bacterial membrane integrity.

2.6. Drug Resistance-Developing Study

On the basis of above excellent antibacterial ability and clear antibacterial mechanism, the development of drug resistance is also evaluated using *S. aureus* as a model. As a comparison, norfloxacin, a conventional antibiotic is utilized. *S. aureus* are treated by antibacterial agents (β -PM-PIO and norfloxacin) with continuous 1/2MIC treatment for 10 generations. Interestingly, MIC for the β -PM-PIO-treated bacteria remains unchanged even at the 10th passage (Figures 5G; Figure S21, Supporting Information). By contrast, a visible increase in the MIC of norfloxacin-treated *S. aureus* is captured at the 6th passage ($\text{MIC} = 0.5 \mu\text{g mL}^{-1}$), which is 5-fold enhancement relative to those of the primary passage ($0.1 \mu\text{g mL}^{-1}$). With the constant treatment to the 10th passage, the MIC significantly increases to 1500-fold ($150 \mu\text{g mL}^{-1}$) that of the previous four generations (Figure S22, Supporting Information). Notably, when the 10th passage of norfloxacin-resistant *S. aureus* is incubated with β -PM-PIO for 16 h, it can also be killed completely at a

concentration of 8 μM (Figure 5H). Better, when white light is applied (40 mW cm^{-2} for 10 min), the norfloxacin-resistant bacteria can be completely suppressed at 5 μM . All of these results indicate that β -PM-PIO does not develop drug-resistant bacteria after multiple treatments, and can effectively kill drug-resistant bacteria at a relatively low concentration.

2.7. Antibiofilm Treatment

Given the antibacterial ability toward planktonic bacteria, the antibiofilm performance of β -PM-PIO is further explored. The MTT assay is employed to quantify the biofilm mass.^[11] As illustrated in Figure 6A, the bacteria are incubated with different concentrations of β -PM-PIO for 30 min and then treated with and without white light (40 mW cm^{-2}) for 10 min. The formation of biofilm is detected after static culture for 24 h at 37 °C. As shown in Figure 6C and 6D, the biofilm biomass is reduced with the increase of β -PM-PIO concentration, and biofilm formation can be completely inhibited at about 5 μM under dark or light conditions. With SYTOX blue as the dead bacterial fluorescence probe, CLSM is also applied to confirm the biofilm

inhibition ability of β -PM-PIO. For these experimental groups, bacteria are incubated with β -PM-PIO (10 μM) for 30 min, and then treated with and without white light (40 mW cm^{-2}) for 10 min, followed by the static culture for 24 h at 37 °C. And for the control group, bacterial are cultured for 24 h without any treatment. Before imaging, β -PM-PIO (5 μM) and SYTOX Blue (5 μM) are added to each petri dish for 10 min at RT. As illustrated in Figure S23A, Supporting Information, a layer of biofilm with red fluorescence from β -PM-PIO is observed for the control group. But for these two experimental groups (Figure 6G; Figure S23B, Supporting Information), merely a few clustered molecules are observed in the CLSM image, as indicated by a few red fluorescence dots. Such obvious comparison demonstrates β -PM-PIO can efficiently inhibit biofilm formation under the synergistic effect of phototoxicity and dark toxicity.

Moreover, the eradication capacity of mature biofilm is also investigated. As shown in Figure 6B, after the formation of mature biofilm, different concentrations of β -PM-PIO are incubated with mature biofilm at 37 °C for 30 min. Then, after treatment with and without white light (40 mW cm^{-2}) for 20 min, MTT assay is conducted to determine the biofilm

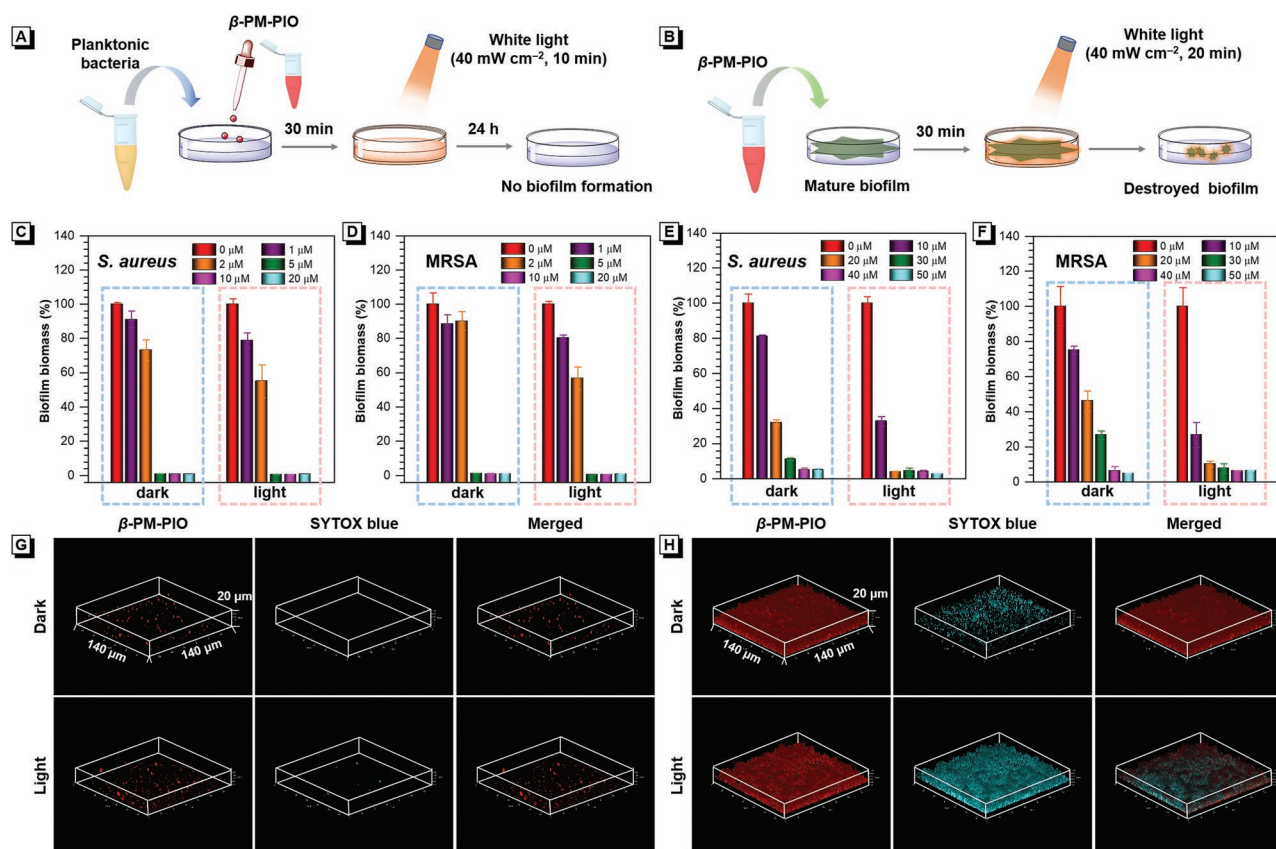


Figure 6. The procedure illustration of biofilm A) formation inhibition and B) destruction by β -PM-PIO. The biofilm biomass of C) *S. aureus* and D) MRSA are incubated with β -PM-PIO with different concentrations for 24 h under dark and light conditions without preincubate (White light: 40 mW cm^{-2} , 10 min). The biofilm biomass of E) *S. aureus* and F) MRSA are incubated with β -PM-PIO with different concentrations under dark and light conditions after 24 h preincubate (White light: 40 mW cm^{-2} , 20 min). G) 3D CLSM imaging of *S. aureus* incubated with β -PM-PIO (10 μM) for 24 h without preincubation (White light: 40 mW cm^{-2} , 10 min). And H) 3D CLSM imaging of *S. aureus* incubated with β -PM-PIO (20 μM) for 30 min after 24 h preincubate (White light: 40 mW cm^{-2} , 20 min) (For SYTOX Blue Dead Cell Stain, $\lambda_{\text{ex}} = 405\text{ nm}$, $\lambda_{\text{em}} = 430\text{--}490\text{ nm}$; and for β -PM-PIO, $\lambda_{\text{ex}} = 488\text{ nm}$, $\lambda_{\text{em}} = 600\text{--}700\text{ nm}$).

biomass. As shown in Figure 6E and 6F, the antibiofilm activity of β -PM-PIO is dose-dependent. And the biofilm biomass can be reduced to less than 10% at 40 μM in dark conditions for both *S. aureus* and MRSA. Better, upon irradiation, β -PM-PIO can achieve 90% biofilm removal at 20 μM . Additionally, the obvious cyan fluorescence signal (SYTOX blue) of the CLSM image further confirms that β -PM-PIO (20 μM) can completely destroy mature biofilm (Figure 6H; Figure S23C, Supporting Information) after irradiation. Such a low concentration of eradicating biofilm with light irradiation may attribute to the efficient destruction of EPS by ROS, which can further accelerate the penetration of β -PM-PIO into the biofilm and continuously generate ROS under light.

2.8. In Vivo Anti-Infected Model

Inspired by the excellent bacterial inactivation of β -PM-PIO in vitro, its anti-infection ability against drug-resistant bacteria in vivo is further evaluated by the MRSA-infected wound model on mice, as displayed in Figure 7A. The infected mice are randomly divided into three groups. For the experimental group, the infected regions of the mice are exposed to white

light (60 mW cm^{-2}) for 10 min after treatment with 100 μL β -PM-PIO (5 μM) for 30 min in dark. For comparison, anti-infection treatment using intramuscularly injected benzylpenicillin (Penicillin, 2400 unit) is employed. Here, Penicillin, an antimicrobial agent that is commonly used in clinical. And for the blank group, the infected regions are incubated with 100 μL PBS without any post-treatment.

The macroscopic appearance of the wound-healing process is recorded at different time points. As shown in Figure 7B and 7C, the infected wound size gradually decreases with the extension of the treatment period for the experimental group and is smaller than those in Penicillin- and PBS-treated groups, revealing the excellent anti-infection ability of β -PM-PIO. In addition, the hematoxylin and eosin (H&E) staining indicates that the wound tissues of infected mice treated by β -PM-PIO with white light irradiation have better tissue recovery and there are no noticeable damaged cells with infiltrating inflammatory cells as compared to other groups (Figure 7E). What is more, fluorescence imaging of CD45 (leukocyte common antigen) and DAPI (nuclear dye) unambiguously confirms that β -PM-PIO can effectively inhibit bacterial growth without inducing inflammatory lesions and cell death in mammals (Figure 7F). Meanwhile,

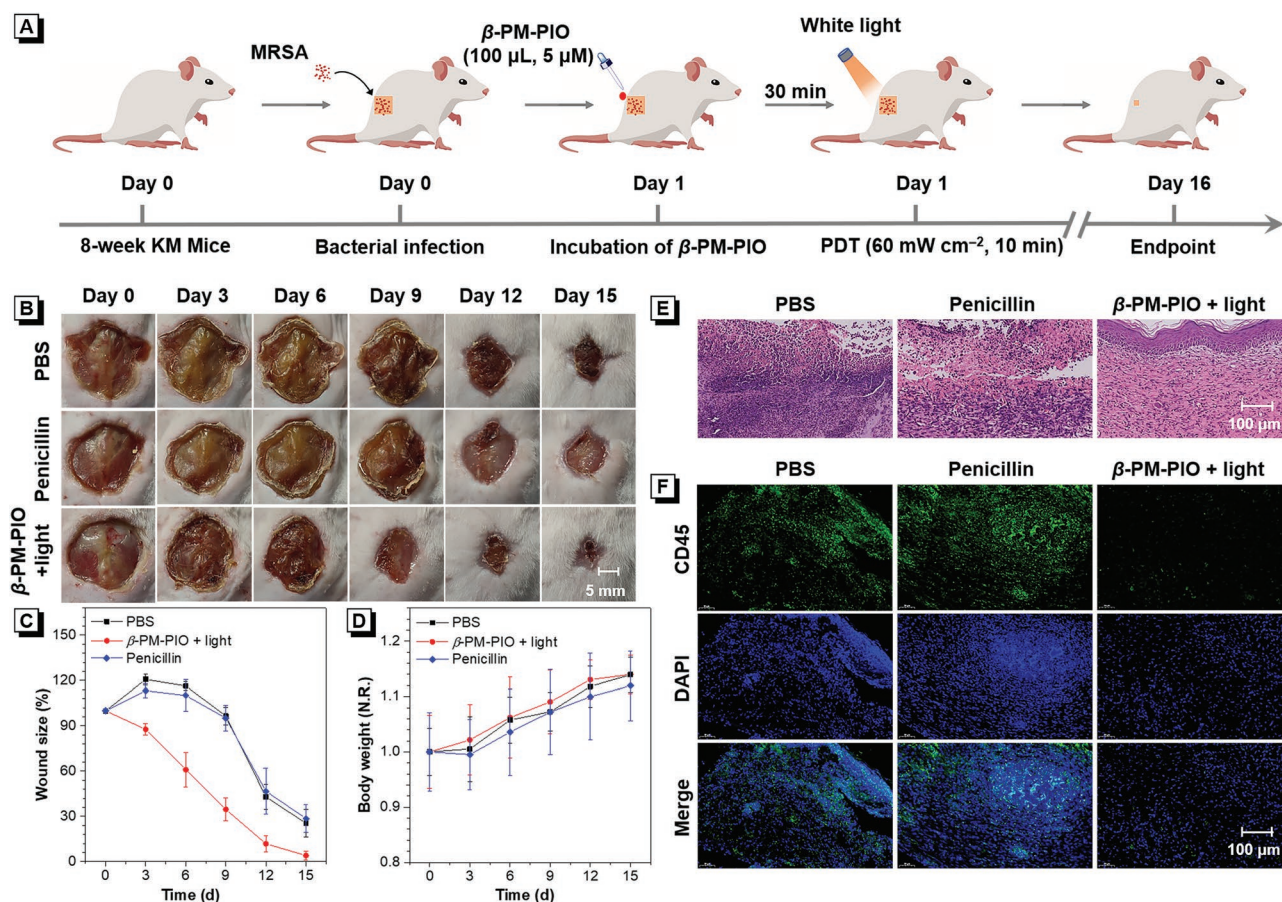


Figure 7. A) Schematic diagram of the establishment of MRSA-infected wound model on mice and in vivo anti-infection treatment of β -PM-PIO. B) Photographs of the wounds during the healing process after different treatments. The diagrams of C) wound size and D) bodyweight during the wound healing process after different treatments. E) H&E staining images and F) fluorescence imaging of CD45 and DAPI to the wound slices after different treatments.

two major bacterial infectious biomarkers (Blood leukocytes and Neutrophile granulocyte) in the blood of mice with different treatments on the 15th day are monitored. As shown in Figure S24, Supporting Information, the level of these two biomarkers for the experimental group is lower, indicating the inflammatory reaction level in the β -PM-PIO-treated group is remarkably reduced, relative to the other two groups. The above results indicate that β -PM-PIO has superior performance in antimicrobial therapy and can significantly promote the wound-healing process.

2.9. Biocompatibility

The toxicity evaluation of β -PM-PIO in vitro is carried out with the standard method of the 3-(4,5-dimethylthiazol-2-yl)-2,5-diphenyltetrazolium bromide (MTT) assay by using HeLa cell as a cell model. As illustrated in Figure S25, Supporting Information, the cell viability remains nearly 90%, after being treated with 50 μ M β -PM-PIO for 12 or 16 h without light illumination, disclosing its negligible dark toxicity to living cells. The biosafety of β -PM-PIO on mice is also evaluated. As displayed in Figure 7D, the bodyweight of the infected mice remains unchanged during the healing process after treatments. Eventually, H&E staining of different organs (heart, liver, spleen, lung, and kidney) of mice is also performed (Figure S26, Supporting Information), which shows no noticeable organ damage. The above results verify that β -PM-PIO possesses reliable biocompatibility in the treatment of MRSA infection.

3. Conclusion

In summary, a tailor-made PIO-based antibacterial agent (β -PM-PIO) is successfully developed. The precision molecular design facilitates the β -PM-PIO with AIE character and high ROS generation ability. Theoretical results indicate that its excellent $^1\text{O}_2$ generation ability results from the small ΔE_{ST} , considerable SOC value, and sufficiently high T_1 energy level. The in vitro test demonstrates that β -PM-PIO possesses image-guided targeting ability towards *S. aureus* and MRSA. Better, with the special mechanism of bacterial membrane destruction, β -PM-PIO can successfully kill bacteria with less potential of developing drug resistance. Additionally, β -PM-PIO can also function efficiently in biofilm imaging, inhibition of biofilm formation, and eradication of mature biofilm. These superb antibacterial and antibiofilm performances are attributed to the synergistic effect of strong phototoxicity and dark toxicity to bacteria. Remarkably, in vivo experiment verifies that it can effectively treat resistant-bacterial infection and promote the recovery of infected wounds while maintaining excellent biocompatibility with negligible dark toxicity to living cells and tissues. Collectively, these results demonstrate β -PM-PIO holds great potentials in the treatment of "super bacteria." This work also provides an efficient strategy for the treatment of biofilm-associated infection, and the clinical therapeutic effect remains to be investigated in further researches.

Supporting Information

Supporting Information is available from the Wiley Online Library or from the author.

Acknowledgements

J.L. and Z.M. contributed equally to this work. This research was financially supported by the National Natural Science Foundation of China (21788102) and the Natural Science Foundation of Guangdong Province (2019B030301003). The ethics of animal experiments were approved by the Ethics Committee of Tongji Hospital, Tongji Medical College of Huazhong University of Science and Technology (TJH-201903002).

Conflict of Interest

The authors declare no conflict of interest.

Data Availability Statement

The data that support the findings of this study are available from the corresponding author upon reasonable request.

Keywords

bacterial infection, biofilms, cationic photosensitizers, drug-resistance bacteria, phosphindole oxides

Received: February 3, 2022

Revised: February 28, 2022

Published online:

- [1] a) S. DeWeerd, *Nature* **2015**, 521, S10; b) R. F. Schwabe, C. Jobin, *Nat. Rev. Cancer* **2013**, 13, 800.
- [2] a) C. Willyard, *Nature* **2017**, 543, 15; b) L. Váradi, J. L. Luo, D. E. Hibbs, J. D. Perry, R. J. Anderson, S. Orega, P. W. Groundwater, *Chem. Soc. Rev.* **2017**, 46, 4818; c) F. Naz, *Lancet Infect. Dis.* **2013**, 13, 70318; d) M. Frieri, K. Kumar, A. Boutin, *J. Infect. Public Health* **2017**, 10, 369; e) C. D. Sally, F. Tom, W. John, M. L. David, W. David, *Lancet* **2013**, 381, 1606.
- [3] a) D. Davies, *Nat. Rev. Drug Discovery* **2003**, 2, 114; b) A. Penesyan, M. Gillings, I. T. Paulsen, *Molecules* **2015**, 20, 5286.
- [4] a) N. Høiby, T. Bjørnsholt, M. Givskov, S. Molin, O. Ciofu, *Int. J. Antimicrob. Agents* **2010**, 35, 332; b) W. Xiu, J. Shan, K. Yang, H. Xiao, L. Yuwen, L. Wang, *View* **2021**, 2, 20200065.
- [5] R. Roy, M. Tiwari, G. Donelli, V. Tiwari, *Virulence* **2018**, 9, 522.
- [6] E. K. Ampofo, I. K. Amponsah, E. Asante-Kwatia, F. A. Armah, P. K. Atchoglo, A. Y. Mensah, *Adv. Pharm. Pharm. Sci.* **2020**, 2020, 8821905.
- [7] F. Reffuveille, C. d. I. Fuente-Núñez, S. Mansour, R. E. W. Hancock, *Antimicrob. Agents. Ch.* **2014**, 58, 5363.
- [8] J. Parisot, S. Carey, E. Breukink, W. C. Chan, A. Narbad, B. Bonev, *Antimicrob. Agents. Ch.* **2008**, 52, 612.
- [9] a) S. Panja, R. Bharti, G. Dey, N. A. Lynd, S. Chattopadhyay, *ACS Appl. Mater. Interfaces* **2019**, 11, 33599; b) A. Punia, K. Lee, E. He, S. Mukherjee, A. Mancuso, P. Banerjee, N.-L. Yang, *Int. J. Mol. Sci.* **2015**, 16, 23867.

- [10] a) I. D. Peltan, S. M. Brown, J. R. Bledsoe, J. Sorensen, M. H. Samore, T. L. Allen, C. L. Hough, *Chest* **2019**, 155, 938; b) M. N. Melo, R. Ferre, M. A. R. B. Castanho, *Nat. Rev. Microbiol.* **2009**, 7, 245; c) H. Sun, Y. Hong, Y. Xi, Y. Zou, J. Gao, J. Du, *Biomacromolecules* **2018**, 19, 1701.
- [11] J. Sun, M. Li, M. Lin, B. Zhang, X. Chen, *Adv. Mater.* **2021**, 33, 2104402.
- [12] Y. Sun, H. Qin, Z. Yan, C. Zhao, J. Ren, X. Qu, *Adv. Funct. Mater.* **2019**, 29, 1808222.
- [13] P. Agostinis, K. Berg, K. A. Cengel, T. H. Foster, A. W. Girotti, S. O. Gollnick, S. M. Hahn, M. R. Hamblin, A. Juzeniene, D. Kessel, M. Korbelik, J. Moan, P. Mroz, D. Nowis, J. Piette, B. C. Wilson, J. Golab, *CA: Cancer J. Clin.* **2011**, 61, 250.
- [14] G. B. Kharkwal, S. K. Sharma, Y. Y. Huang, T. H. Dai, M. R. Hamblin, *Lasers Surg. Med.* **2011**, 43, 755.
- [15] a) J. Li, Z. Zhuang, Z. Zhao, B. Z. Tang, *VIEW* **2022**, 3, 20200121; b) Z. Zhou, J. Song, L. Nie, X. Chen, *Chem. Soc. Rev.* **2016**, 45, 6597.
- [16] a) J. Dai, X. Wu, S. Ding, X. Lou, F. Xia, S. Wang, Y. Hong, *J. Med. Chem.* **2020**, 63, 1996; b) G. Feng, G.-Q. Zhang, D. Ding, *Chem. Soc. Rev.* **2020**, 49, 8179; c) L. Yang, X. Wang, G. Zhang, X. Chen, G. Zhang, J. Jiang, *Nanoscale* **2016**, 8, 17422; d) Y. Cui, R. Zhang, L. Yang, S. Lv, *Chinese Chem. Lett.* **2019**, 30, 1078; e) J. Dai, Y. Cheng, J. Wu, Q. Wang, W. Wang, J. Yang, Z. Zhao, X. Lou, F. Xia, S. Wang, B. Z. Tang, *ACS Nano* **2020**, 14, 14698.
- [17] a) G. Qi, F. Hu, Kenry, K. C. Chong, M. Wu, Y. H. Gan, B. Liu, *Adv. Funct. Mater.* **2020**, 30, 2001338; b) X. Shi, S. H. P. Sung, J. H. C. Chau, Y. Li, Z. Liu, R. T. K. Kwok, J. Liu, P. Xiao, J. Zhang, B. Liu, J. W. Y. Lam, B. Z. Tang, *Small Methods* **2020**, 4, 2000046.
- [18] a) J. Dai, Y. Li, Z. Long, R. Jiang, Z. Zhuang, Z. Wang, Z. Zhao, X. Lou, F. Xia, B. Z. Tang, *ACS Nano* **2020**, 14, 854; b) J. Dai, M. Wu, Q. Wang, S. Ding, X. Dong, L. Xue, Q. Zhu, J. Zhou, F. Xia, S. Wang, Y. Hong, *Natl. Sci. Rev.* **2021**, 8, nwab039; c) R. Jiang, J. Dai, X. Dong, Q. Wang, Z. Meng, J. Guo, Y. Yu, S. Wang, F. Xia, Z. Zhao, X. Lou, B. Z. Tang, *Adv. Mater.* **2021**, 33, 2101158; d) H. Chen, S. Li, M. Wu, Kenry, Z. H., C.-S. Lee, B. Liu, *Angew. Chem., Int. Ed.* **2020**, 59, 632.
- [19] a) B. Wang, H. Wu, R. Hu, X. Liu, Z. Liu, Z. Wang, A. Qin, B. Z. Tang, *Adv. Healthcare Mater.* **2021**, 10, 2100136; b) J. Xia, W. Wang, X. Hai, S. E. Y. Shu, J. Wang, *Chinese Chem. Lett.* **2019**, 30, 421; c) F. Xiao, B. Cao, L. Wen, Y. Su, M. Zhan, L. Lu, X. Hu, *Chinese Chem. Letters* **2020**, 31, 2516; d) T. Zhou, R. Hu, L. Wang, Y. Qiu, G. Zhang, Q. Deng, H. Zhang, P. Yin, B. Situ, C. Zhan, A. Qin, B. Z. Tang, *Angew. Chem., Int. Ed.* **2020**, 59, 9952.
- [20] Z. Zhuang, J. Dai, M. Yu, J. Li, P. Shen, R. Hu, X. Lou, Z. Zhao, B. Z. Tang, *Chem. Sci.* **2020**, 11, 3405.
- [21] S. Zhao, W. Huang, C. Wang, Y. Wang, Y. Zhang, Z. Ye, J. Zhang, L. Deng, A. Dong, *Biomacromolecules* **2020**, 21, 5269.
- [22] J. Jia, C. Hu, Y. Cui, Y. Li, W. Wang, L. Han, Y. Li, J. Gao, *Dyes Pigm.* **2018**, 149, 843.
- [23] a) H. Tanaka, K. Shizu, H. Nakanotani, C. Adachi, *Chem. Mater.* **2013**, 25, 3766; b) S. Liu, X. Zhou, H. Zhang, H. Ou, J. W. Y. Lam, Y. Liu, L. Shi, D. Ding, B. Z. Tang, *J. Am. Chem. Soc.* **2019**, 141, 5359.
- [24] Y. Tu, Z. Zhao, J. W. Y. Lam, B. Z. Tang, *Natl. Sci. Rev.* **2021**, 8, nwaa260.
- [25] X. Chen, Z. Zhong, Z. Xu, L. Chen, Y. Wang, *Free Radical Res.* **2010**, 44, 587.
- [26] K.-i. Setsukinai, Y. Urano, K. Kakinuma, H. J. Majima, T. Nagano, *J. Biol. Chem.* **2003**, 278, 3170.
- [27] a) T. Entradas, S. Waldron, M. Volk, *J. Photochem. Photobiol. B* **2020**, 204, 111787; b) N. A. Kuznetsova, N. S. Gretsova, O. A. Yuzhakova, V. M. Negrimovskii, O. L. Kaliya, E. A. Luk'yanets, *Russ. J. Gen. Chem.* **2001**, 71, 36.
- [28] M. Lan, S. Zhao, Y. Xie, J. Zhao, L. Guo, G. Niu, Y. Li, H. Sun, H. Zhang, W. Liu, J. Zhang, P. Wang, W. Zhang, *ACS Appl. Mater. Interfaces* **2017**, 9, 14590.
- [29] a) T. Lu, F. Chen, *J. Comput. Chem.* **2012**, 33, 580; b) W. Humphrey, A. Dalke, K. Schulten, *J. Mol. Graphics* **1996**, 14, 33; c) H. Lin, D. G. Truhlar, *Theor. Chem. Acc.* **2007**, 117, 185.
- [30] a) M. A. El-Sayed, *J. Chem. Phys.* **1963**, 38, 2834; b) J. Guo, J. Dai, X. Peng, Q. Wang, S. Wang, X. Lou, F. Xia, Z. Zhao, B. Z. Tang, *ACS Nano* **2021**, 15, 20042.
- [31] a) S. Xu, Y. Yuan, X. Cai, C.-J. Zhang, F. Hu, J. Liang, G. Zhang, D. Zhang, B. Liu, *Chem. Sci.* **2015**, 6, 5824; b) Z. Yang, Z. Zhang, Z. Lei, D. Wang, H. Ma, B. Z. Tang, *ACS Nano* **2021**, 15, 7328; c) J. Zhao, W. Wu, J. Sun, S. Guo, *Chem. Soc. Rev.* **2013**, 42, 5323.
- [32] a) Y. Nosaka, A. Y. Nosaka, *Chem. Rev.* **2017**, 117, 11302; b) A. B. Ormond, H. S. Freeman, *Materials* **2013**, 6, 817.
- [33] R. Hu, F. Zhou, T. Zhou, J. Shen, Z. Wang, Z. Zhao, A. Qin, B. Z. Tang, *Biomaterials* **2018**, 187, 47.
- [34] a) H. Bai, W. He, J. H. C. Chau, Z. Zheng, R. T. K. Kwok, J. W. Y. Lam, B. Z. Tang, *Biomaterials* **2021**, 268, 120598; b) Y. Huang, W. Chen, J. Chung, J. Yin, J. Yoon, *Chem. Soc. Rev.* **2021**, 50, 7725; c) M. M. S. Lee, W. Xu, L. Zheng, B. Yu, A. C. S. Leung, R. T. K. Kwok, J. W. Y. Lam, F.-J. Xu, D. Wang, B. Z. Tang, *Biomaterials* **2020**, 230, 119582.
- [35] X. Chen, L. Huang, Y. Jia, R. Hu, M. Gao, L. Ren, B. Z. Tang, *Adv. Opt. Mater.* **2020**, 8, 1902191.
- [36] R. Hu, Q. Deng, Q. Tang, R. Zhang, L. Wang, B. Situ, C. Gui, Z. Wang, B. Z. Tang, *Biomaterials* **2021**, 271, 120725.